Supporting information

1. X-ray diffraction (XRD) analysis

1.1 Experimental

X-ray diffraction (XRD) analysis was performed to examine the crystal structure of ^{6}LiSal powder using an Ultima IV diffractometer (Rigaku Corp., Tokyo, Japan) with Cu Kα radiation in a 2θ-θ set-up; the scan interval and rate were 0.02°/min and 4.0°/min, respectively. Transmission and absorption spectra were acquired with a UV-Vis spectrophotometer (UV-2700, SHIMAZU Corp., Kyoto, Japan) using a quartz cell with a 1 mm optical path length. For evaluation of radiation hardness, an X-ray generator (D2300-HK, Rigaku Corp., Tokyo, Japan) emittingCu Kα radiation operated at 40 kV and 40 mA was used. The dose rate was estimated to be 100 Gy/min at the sample position.

1.2 Results

^{6}LiSal powder, which was precipitated by evaporating the solvent at 60°C, was removed, and the crystalline phase was analyzed with XRD. Figure S1 shows the XRD pattern of ^{6}LiSal powder. The XRD pattern was consistent with that of LiSal monohydrate in a previous study,[1] which indicated that ^{6}LiSal was successfully synthesized from the raw materials $^{6}Li_2CO_3$ and salicylic acid. Subsequently, the XRD pattern of the dehydrated ^{6}LiSal powder obtained by drying ^{6}LiSal monohydrate at 150°C under vacuum was recorded. In addition, a reference

sample was prepared by applying the same dehydration treatment to the commercially available LiSal monohydrate (> 98%; Tokyo Chemical Industry Co., Ltd., Tokyo, Japan), and its XRD pattern was measured. Figure S2 shows the XRD patterns of the dehydrated ^{6}LiSal powder and reference sample. The XRD pattern of the dehydrated ^{6}LiSal powder is consistent with that of the reference sample, which indicates that ^{6}LiSal was successfully synthesized. Figure S3 shows XRD patterns of ^{6}LiSal before and after X-ray irradiation. After 1000 Gy X-ray irradiation, no change was observed in the peak patterns, suggesting that the lithium-6 salicylate can maintain its molecular and crystal structure after X-ray irradiation.

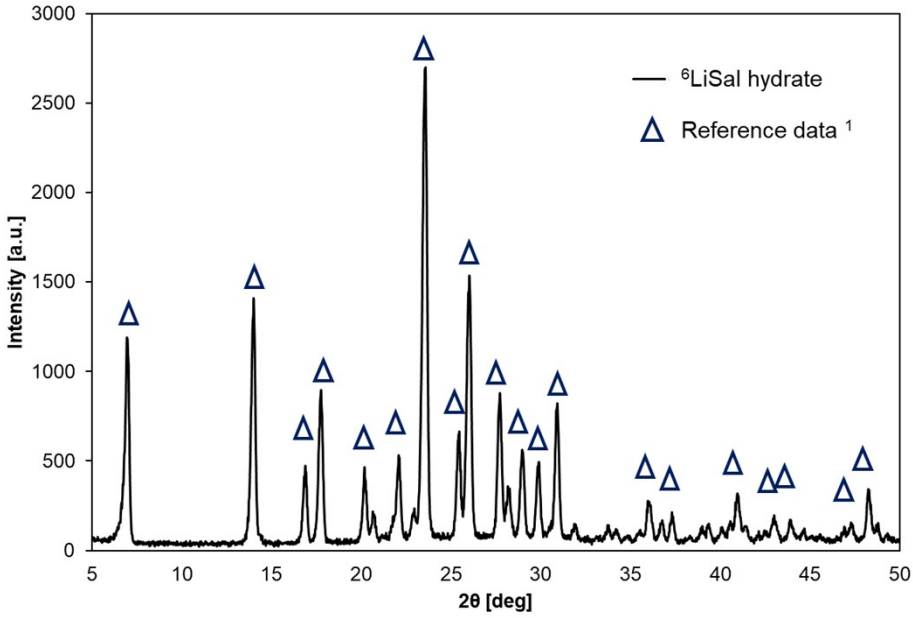

Figure S1. XRD pattern of synthesized lithium-6 salicylate powder.

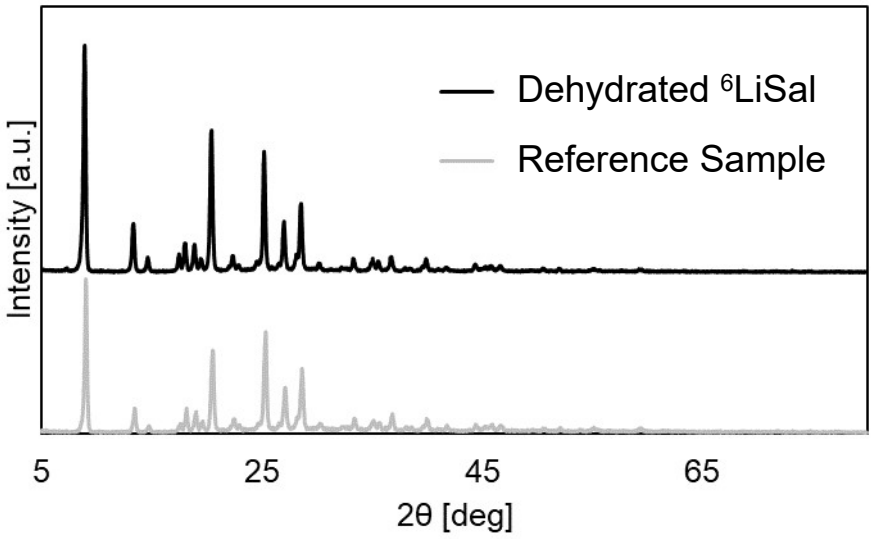

Figure S2. XRD patterns of lithium salicylate powders: dehydrated lithium-6 salicylate and reference sample prepared by dehydrating commercially available lithium salicylate monohydrate.

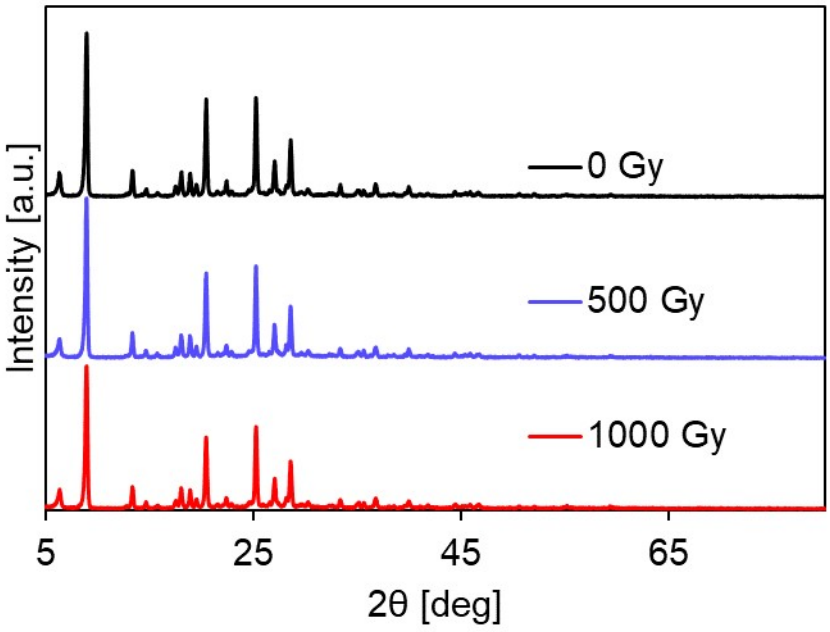

Figure S3. XRD patterns of lithium salicylate powders after X-ray irradiation at different doses of 0, 500, and 1000 Gy.

2. Experimental setup for thermal neutron measurements

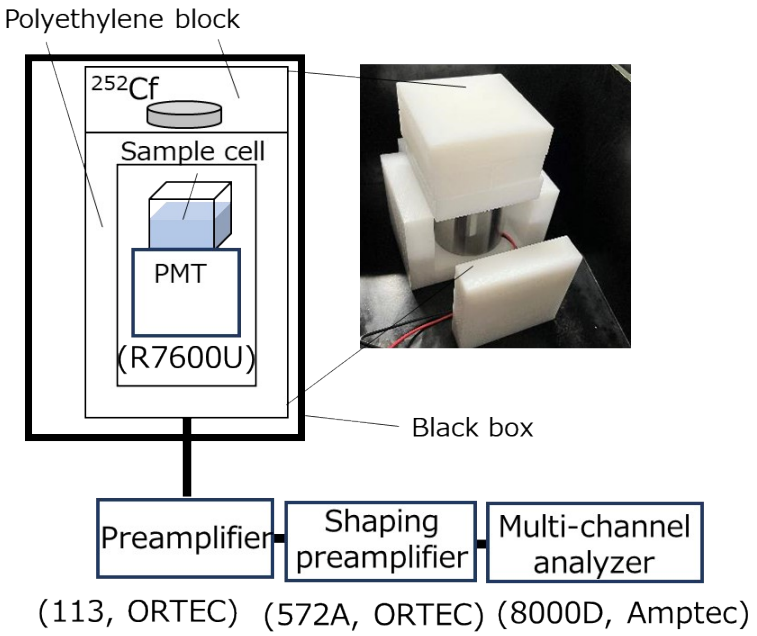

Figure S4. Experimental setup for pulse-height spectra measurements for thermal neutrons with ^{252}Cf source.

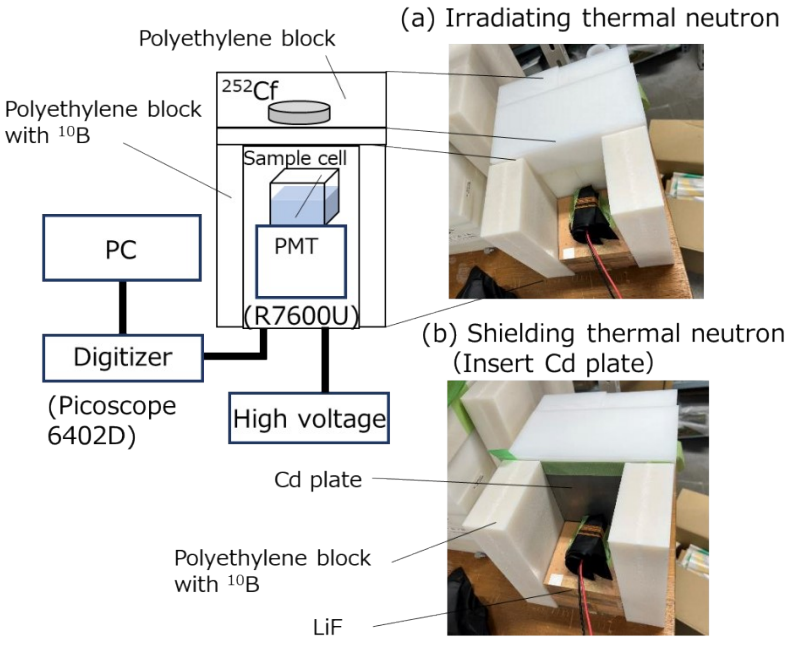

Figure S5. Experimental setup for PSD experiment for (a) irradiating thermal neutron and (b) shielding thermal neutron by inserting a Cd plate between the ^{252}Cf source and the sample cell. To shield fast neutrons scattered from surrounding environments carefully, the sample cell and the PMT were placed on a LiF block and between two ^{10}B-containing polyethylene blocks.

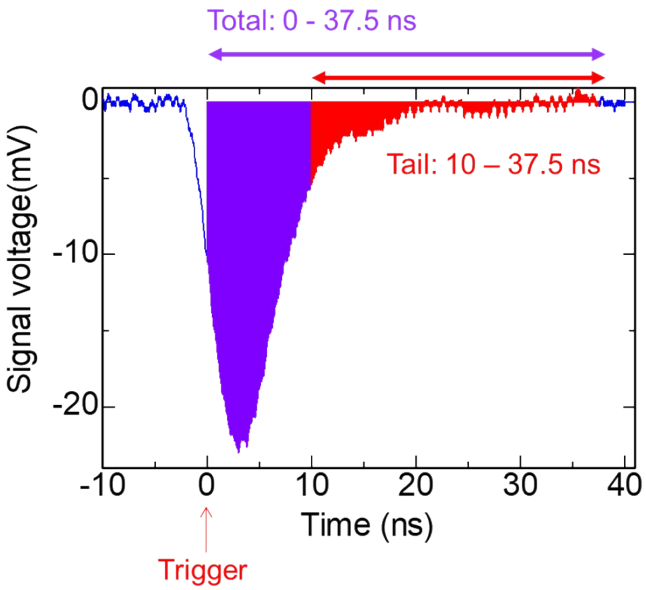

Figure S6. An example of digitized signal pulse shape and definition of total and tail signal: 37.5 ns from trigger channel was set as total signals and 10 to 37.5 ns was set as tail signals.

3.1 Scintillation spectra of mixed solvent samples and references, and plot of PMT sensitivity

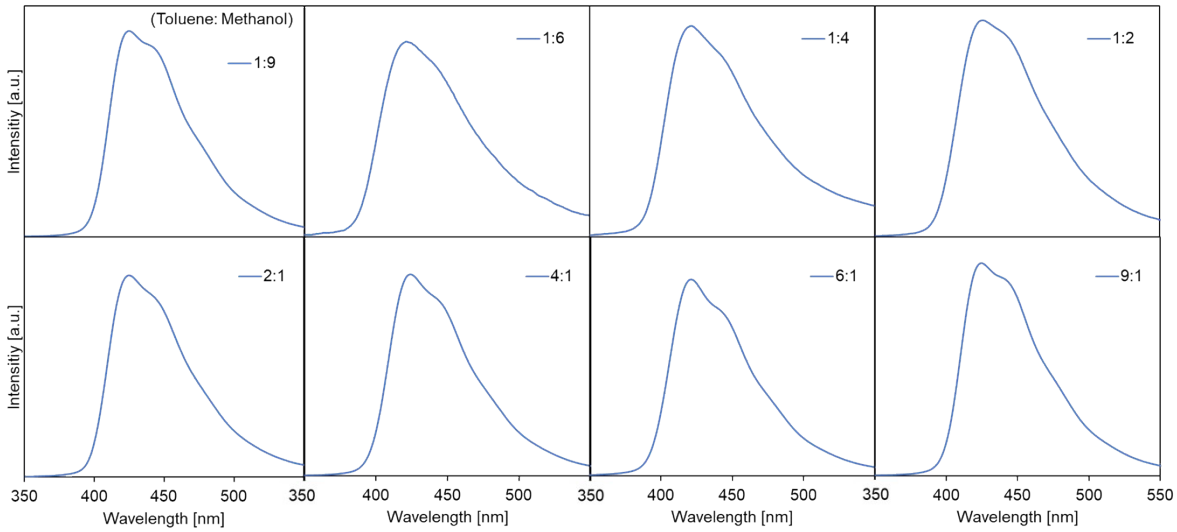

Figure S7. X-ray induced radioluminescence spectra of liquid scintillators mixed with toluene and methanol at 1:9, 1:6, 1:4, 1:2, 2:1, 4:1, 6:1, 9:1.

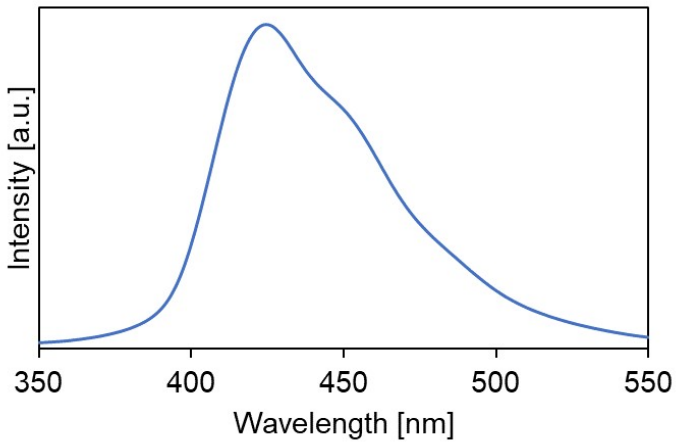

Figure S8. X-ray induced radioluminescence spectrum of NE-142.

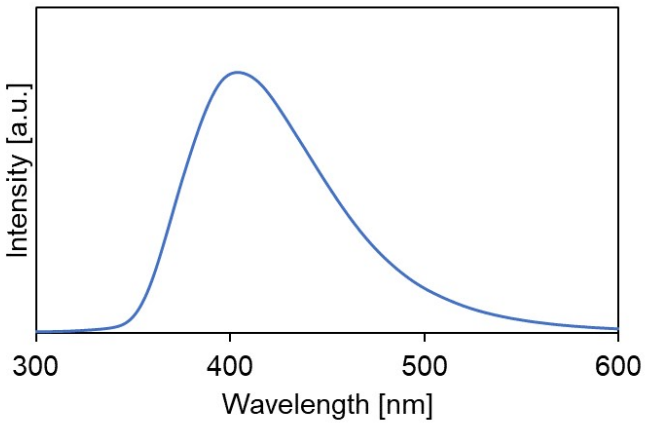

Figure S9. X-ray induced radioluminescence spectrum of Li glass scintillator (GS20).

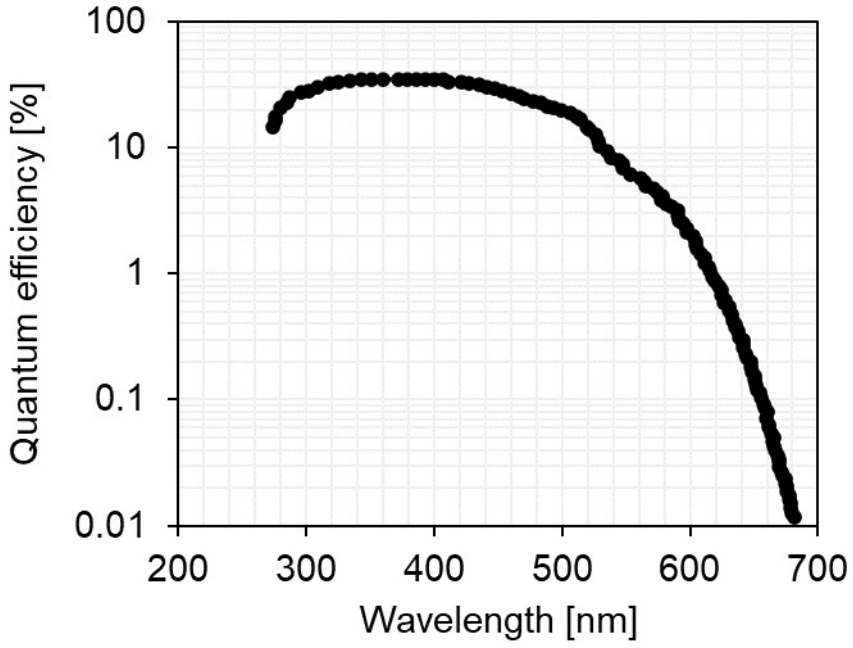

Figure S10. Quantum efficiency response of PMT used in this study.[2]

3.2 Measurement data of samples for phosphor concentration optimization for PSD

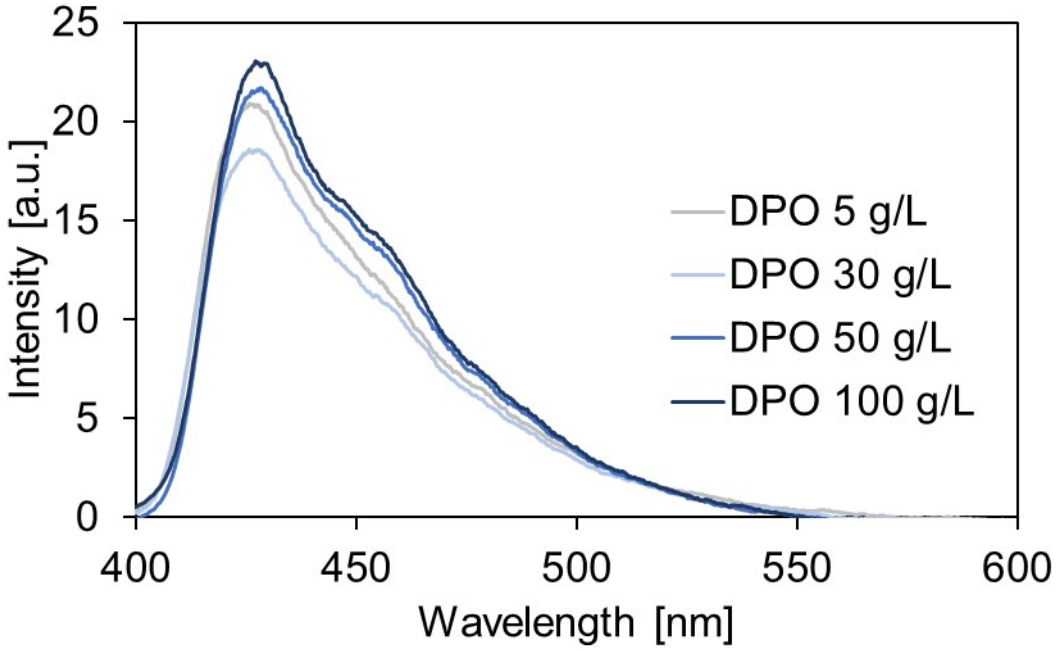

Figure S11. Photoluminescence spectra of lithium-6-loaded liquid scintillators with different DPO concentrations (excited at 255 nm).

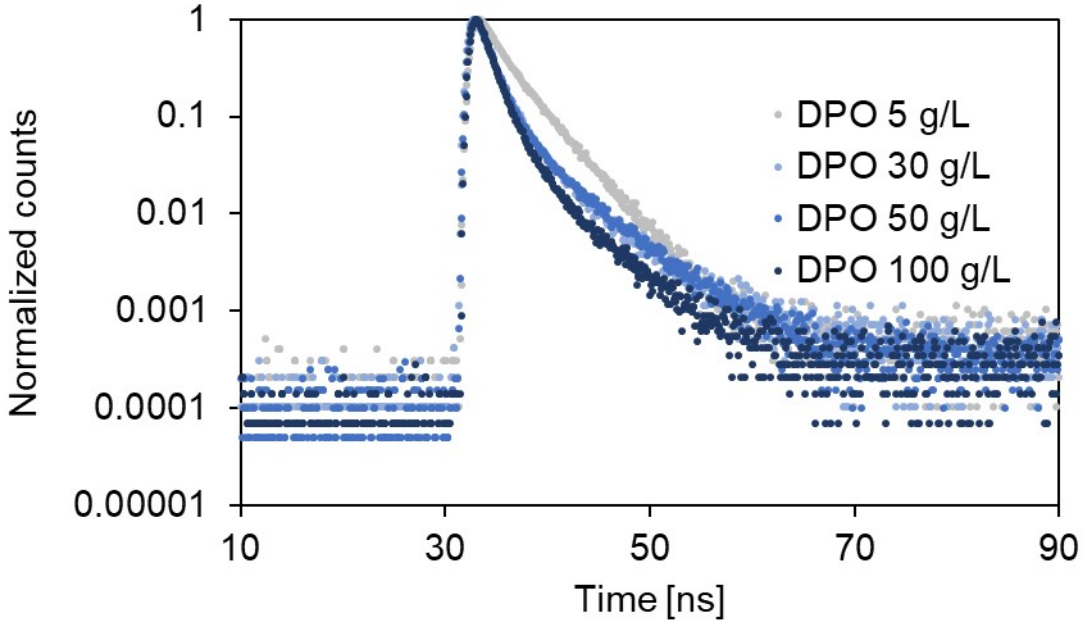

Figure S12. PL temporal profiles of lithium-6-loaded liquid scintillators with different DPO concentrations (λ_{ex} = 255nm, λ_{em} = 425nm).

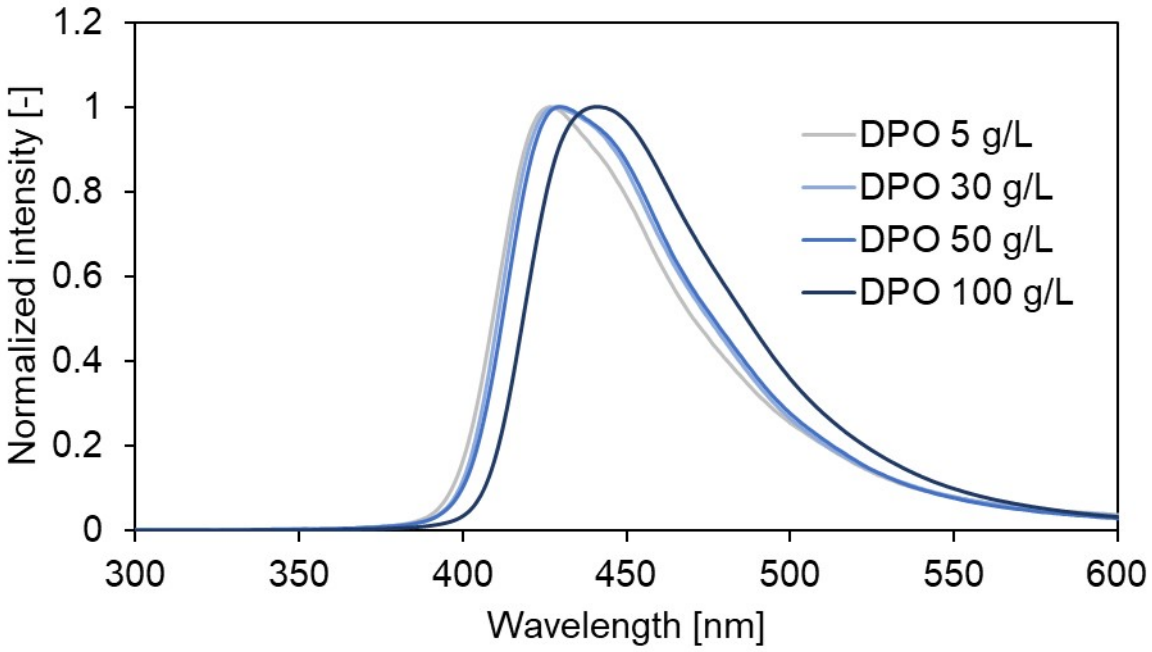

Figure S13. X-ray-induced radioluminescence spectra of lithium-6-loaded liquid scintillators with different DPO concentrations.

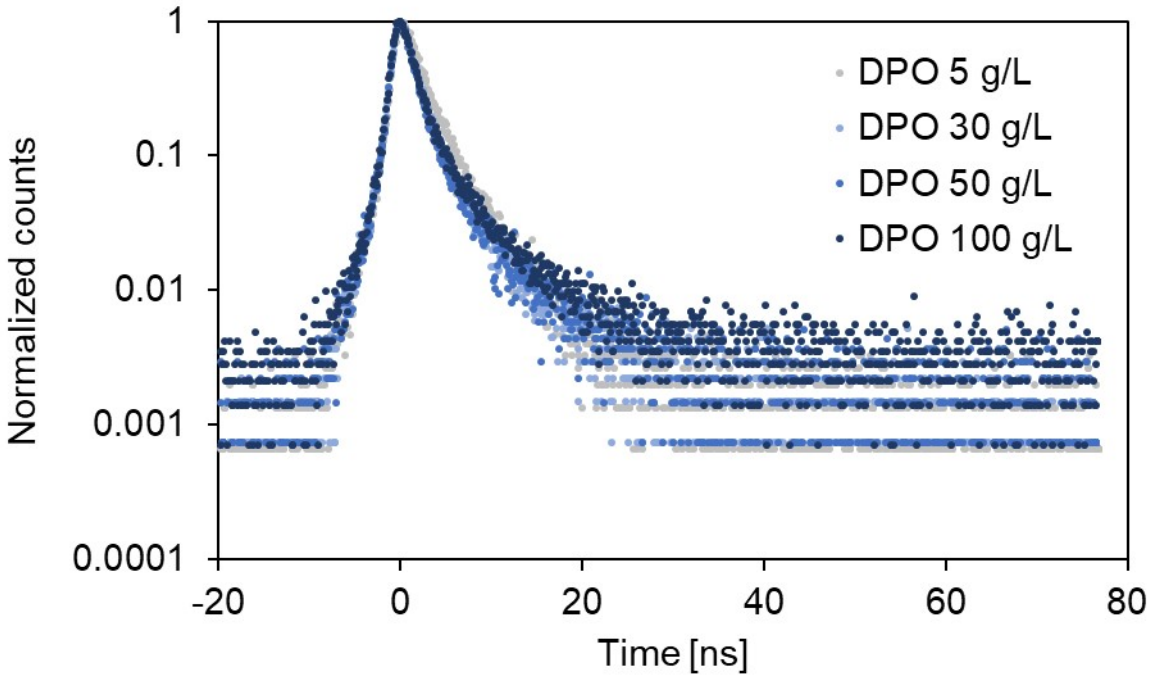

Figure S14. 511 keV gamma ray-irradiated scintillation temporal profiles of lithium-6-loaded liquid scintillators with different DPO concentrations.

3.3 Radiation hardness of ^{6}Li-loaded liquid scintillator

Figure S15 shows the peak intensity of X-ray-induced radioluminescence spectra of the sample with DPO concentration of 5 g/L as a function of cumulative dose. The decrease in intensity was 6.7% after 1500 Gy X-ray irradiation. This result indicates that the fabricated liquid scintillator shows excellent radiation hardness.

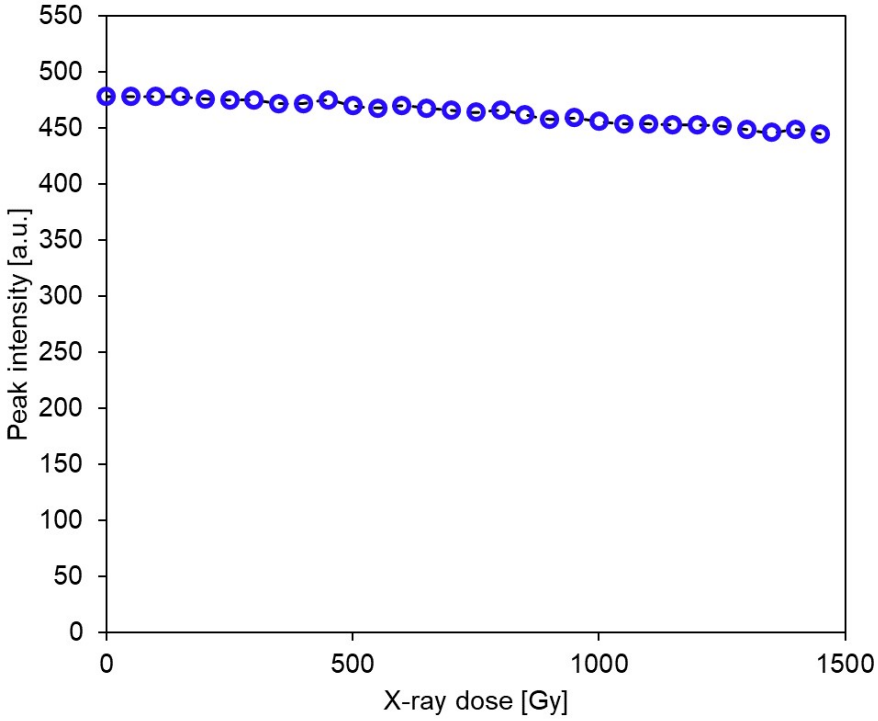

Figure S15 Peak intensity of X-ray-induced radioluminescence spectra of lithium-6-loaded liquid scintillators with 5 g/L of DPO as a function of cumulative dose.

3.4 Pulse shape discrimination measurement

Additionally, other two-dimensional histograms of pulse height were measured by defining the first 17 ns of the peak as the prompt signals and the succeeding 37.5 ns as delayed signals. Two-dimensional histograms of the pulse height were obtained by placing the prompt and delayed signals on the horizontal and vertical axes, respectively. In addition, a control experiment was performed under the condition that the thermal neutrons were completely shielded by inserting a Cd plate between the scintillators and ^{252}Cf source. Figure 6 shows two-dimensional histograms of the pulse height of the ^{6}Li-loaded liquid scintillators. At the lowest DPO concentration of 5 g/L, one aligned set was observed as shown in Figure 6a. This aligned set is a typical gamma-ray signal.[1,3] However, no other signals were observed in this sample. When the DPO concentration was increased to 30 g/L, another spot appeared above the gamma-ray signals. Because thermal neutron events have a higher contribution of slow components than gamma-ray events, the events should appear above the gamma-ray signals. In addition, the spot was not observed in Figure 6e when the thermal neutrons were completely shielded. Thus, we conclude that this spot is derived from a full-energy peak caused by thermal neutron events. Furthermore, as shown in Figure 6b–6d, the thermal neutron events appeared to be separated more clearly from the gamma-ray events by increasing the DPO concentration. This clear separation is attributed to the enhanced contribution of the delayed emission via the TTA process, further supporting that this spot is delivered from thermal neutron events involving a high density of triplet excitations. Consequently, the thermal neutron and gamma-ray events were clearly separated under visual inspection by increasing the DPO concentration to 100 g/L.

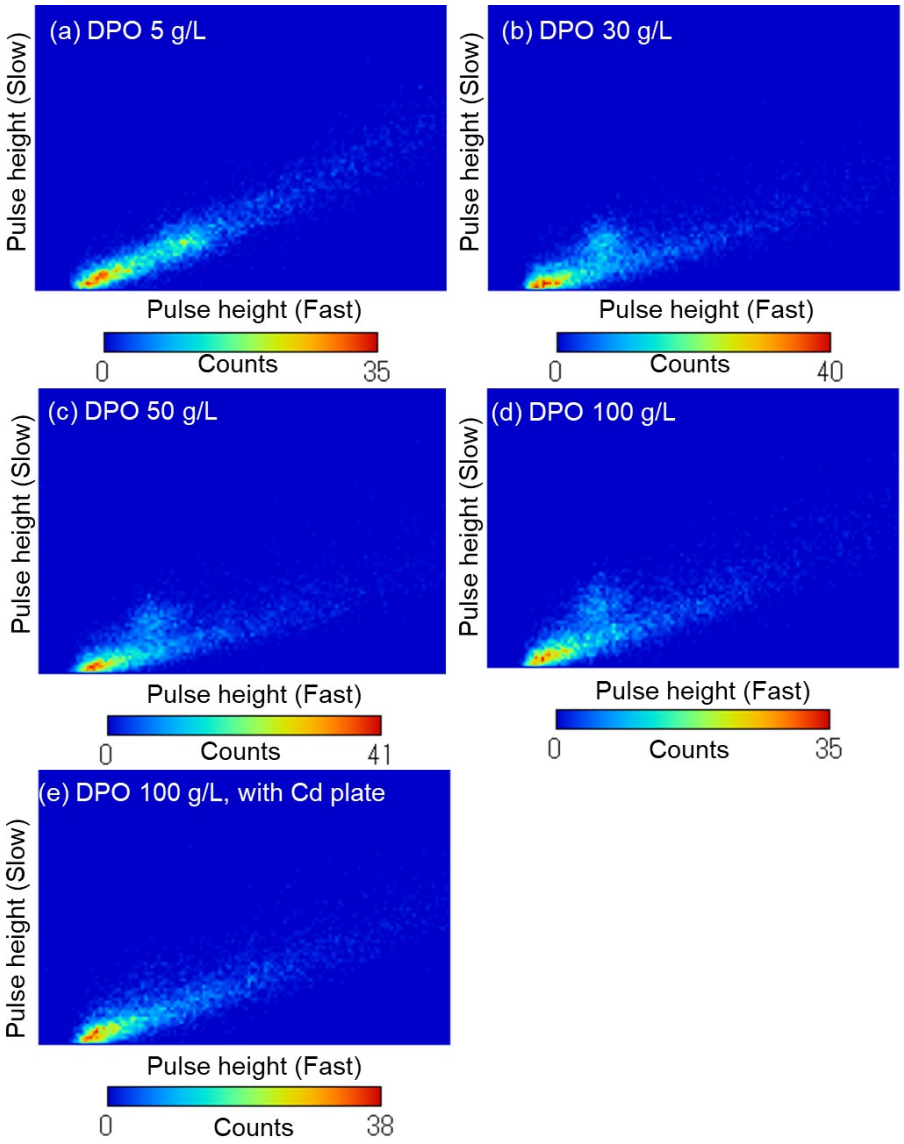

Figure S16. Two-dimensional histograms of the pulse height of lithium-6 salicylate-loaded liquid scintillators with different DPO concentrations: (a) DPO 5 g/L, (b) DPO 30 g/L, (c) DPO 50 g/L, (d) DPO 100 g/L, (e) DPO 100 g/L, a control experiment where thermal neutrons were shielded by a Cd plate.

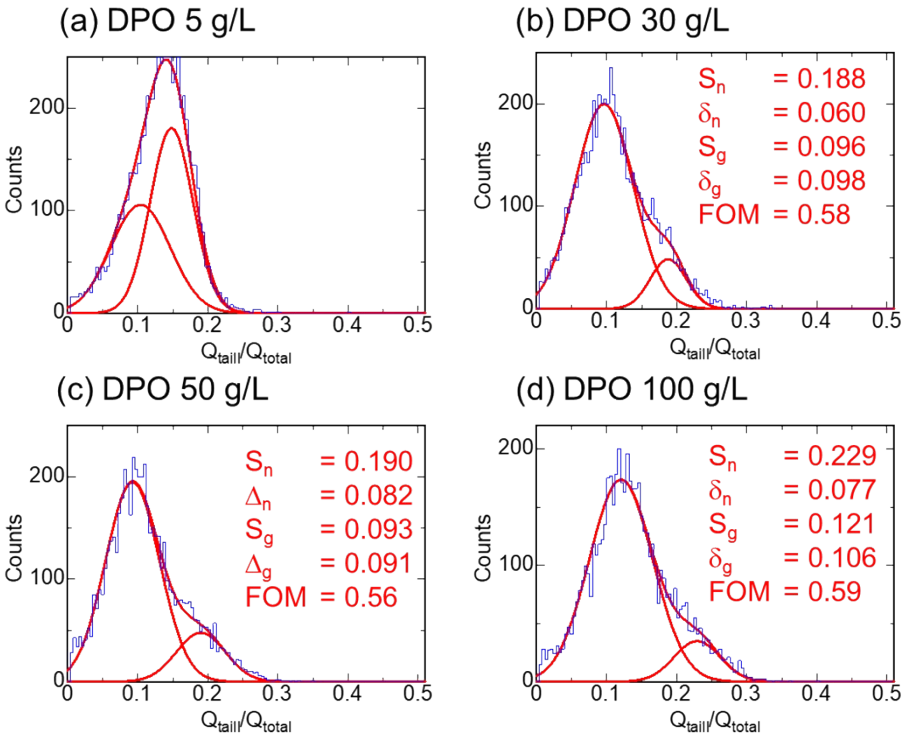

Figure S17. Histograms of neutron events and gamma-ray events of lithium-6 salicylate-loaded liquid scintillators with different DPO concentrations: (a) DPO 5 g/L, (b) DPO 30 g/L, (c) DPO 50 g/L, and (d) DPO 100 g/L.

References

1. N. Zaitseva, J. Newby, G. Hull, C. Saw, L. Carman, N. Cherepy, and S. Payne, Growth and Properties of Lithium Salicylate Single Crystals, *Cryst. Growth Des.*, 2009, **9(8)**, 3799–3802.
2. Hamamatsu Photonics K. K., https://www.hamamatsu.com/jp/en/product/optical-sensors/pmt/pmt_tube-alone/metal-package-type/R7600U.html, (accessed February 14)
3. M. J. I. Balmer, K. A. A. Gamage, and G. C. Taylor, Neutron Assay in Mixed Radiation Fields with a ^{6}Li-Loaded Plastic Scintillator, *J. Instrum.*, 2015, **10(8)**, P08012.